Predicting the HER Activity of SACs on MXenes with Simple Features and Interpretable Machine Learning Models

Supporting Information

Chandra Chowdhury,[1‡] Matteo Lovato,[1,2‡] Giovanni Di Liberto,[1] Francesc Viñes,[2] Francesc Illas,[2] Gianfranco Pacchioni,[1] Livia Giordano*[1]

[1]Department of Materials Science, University of Milano-Bicocca, Via Cozzi 55, 20125 Milano, Italy
[2]Departament de Ciència de Materials i Química Física & Institut de Química Teòrica i Computacional (IQTCUB), Universitat de Barcelona, c/ Martí i Franquès 1-11, 08028 Barcelona, Spain

[‡] These authors contributed equally

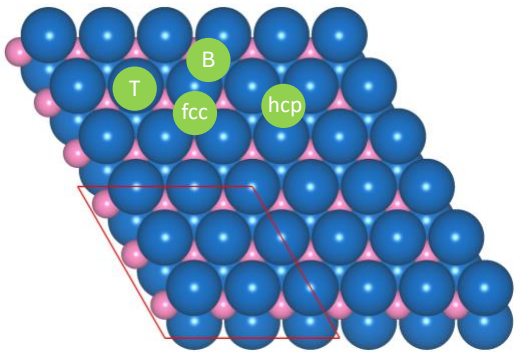

Figure S1. The considered four different high symmetry sites of the M_2C (0001) MXenes surface: the atop site (T) where the adatom is placed directly above an M surface atom, the bridge site (B) corresponding to the midpoint of the M−M bond, and two hollow sites that correspond to carbon (*hcp*) and empty (*fcc*) sites.

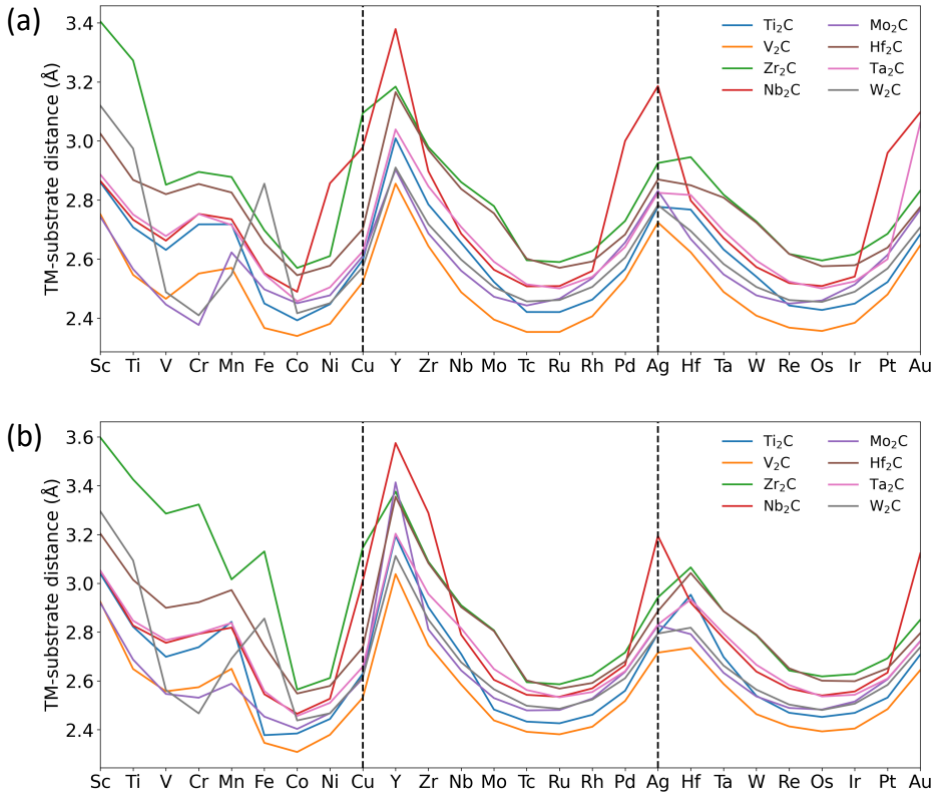

Figure S2. Average distance between the TM and the nearest neighbor atoms of the M_2C (0001) MXenes substrate (TM = Sc, Ti, V, Cr, Mn, Fe, Co, Ni, Cu, Y, Zr, Nb, Tc, Mo, Ru, Rh, Pd, Ag, Hf, Ta, W, Re, Os, Ir, Pt, and Au; M = Ti, V, Zr, Nb, Mo, Hf, Ta, and W) before (a) and after (b) the adsorption of H. Vertical lines separate the three transition metal series.

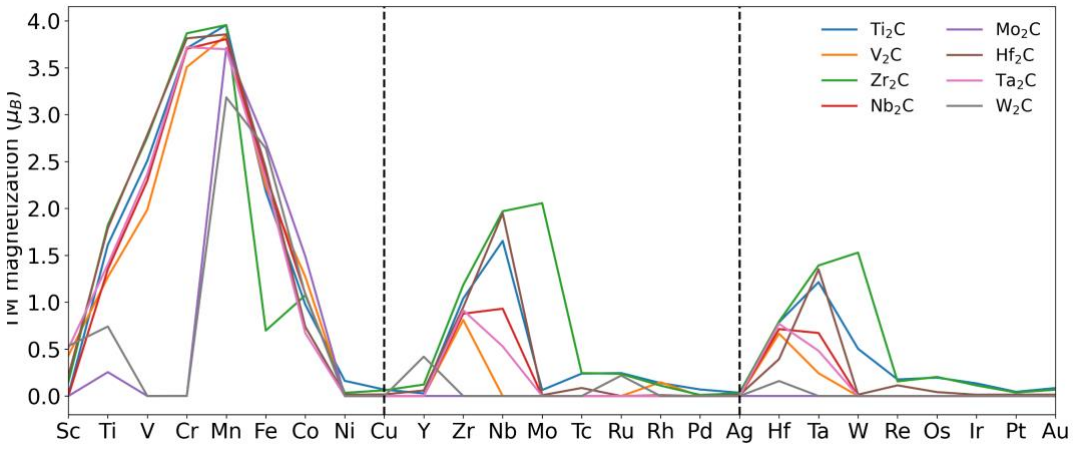

Figure S3. Spin density estimate of the absolute value of the of magnetization of TM adsorbed the M_2C (0001) MXenes substrate (TM = Sc, Ti, V, Cr, Mn, Fe, Co, Ni, Cu, Y, Zr, Nb, Tc, Mo, Ru, Rh, Pd, Ag, Hf, Ta, W, Re, Os, Ir, Pt, and Au; M = Ti, V, Zr, Nb, Mo, Hf, Ta, and W). Vertical lines separate the three transition metal series.

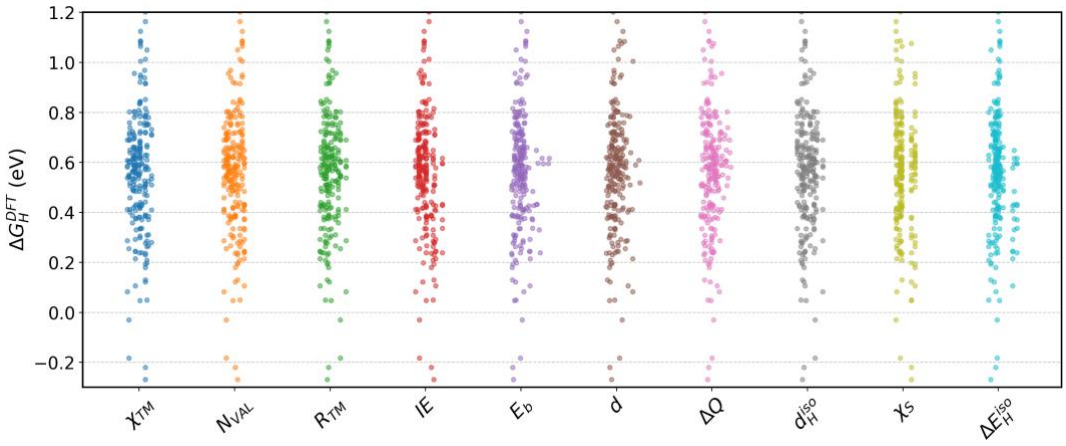

Figure S4: Correlations of individual features with the DFT-calculated ΔG_H values. From the figure it is evident that there is not any strong predictive power of any of the individual features with the target namely, ΔG_H.

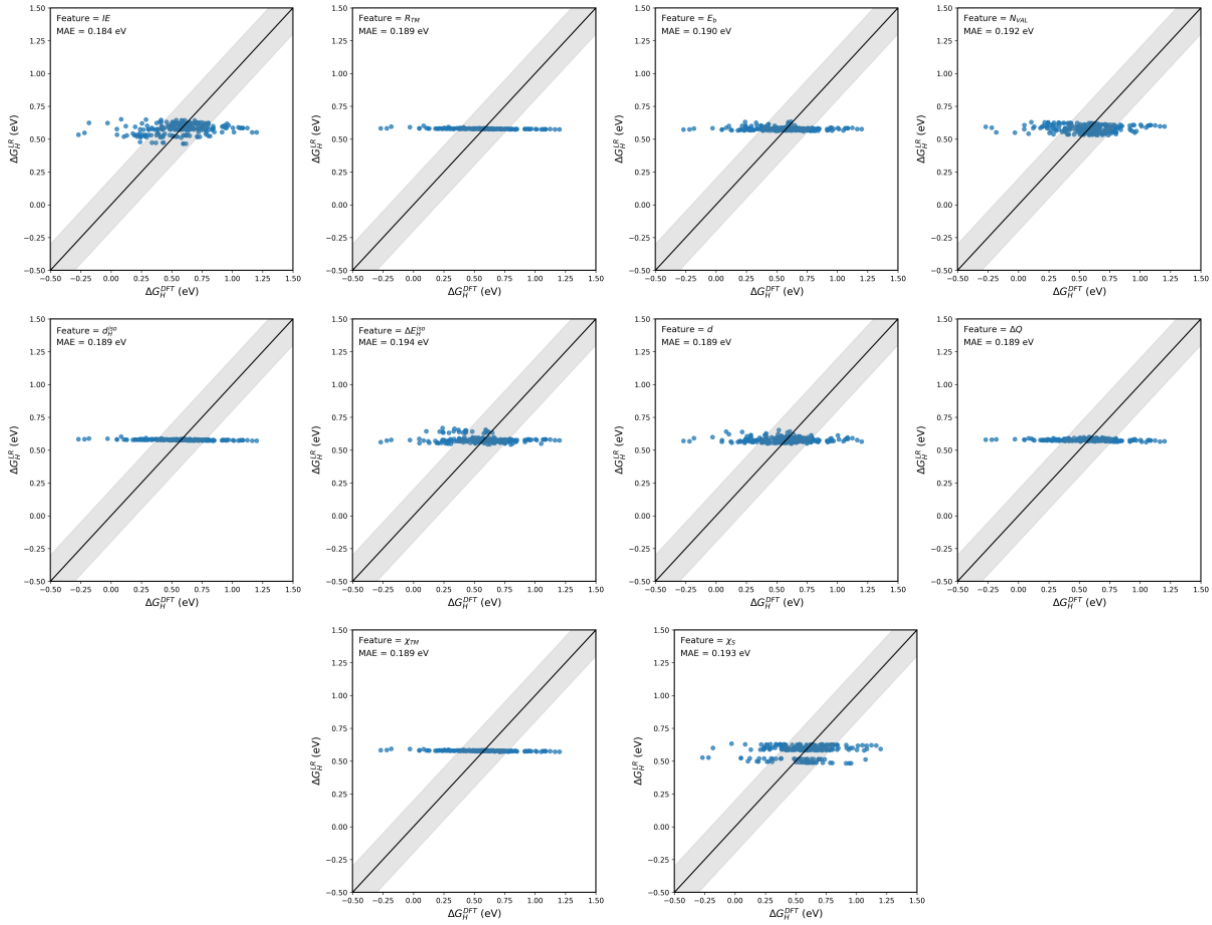

Figure S5. Parity plot for single variable linear regression models for ΔG_H as a function of the different features considered in this work.

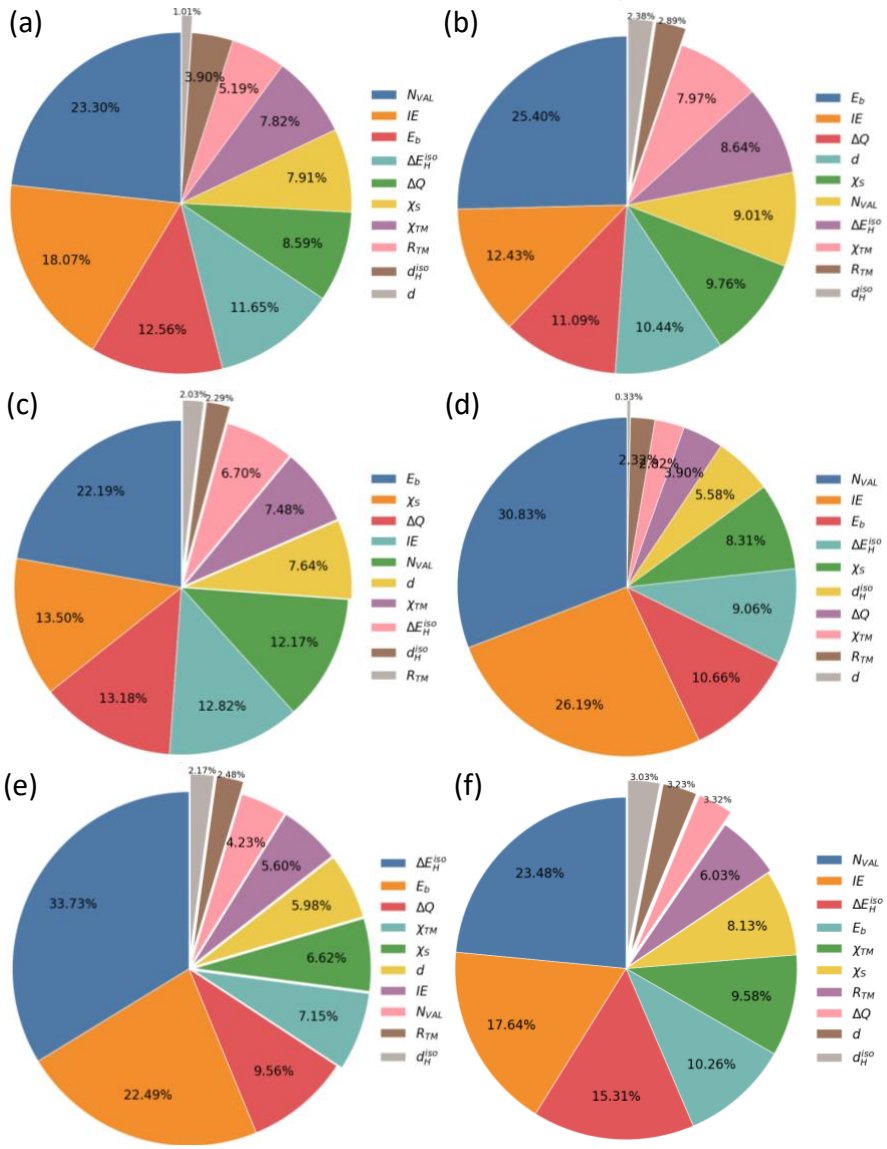

Figure S6: Feature importance analysis for (a) Ridge regression (b) Random Forest, (c) Decision Trees, (d) Extra Trees, (e) AdaBoost and (f) Extra Gradient Boost models.

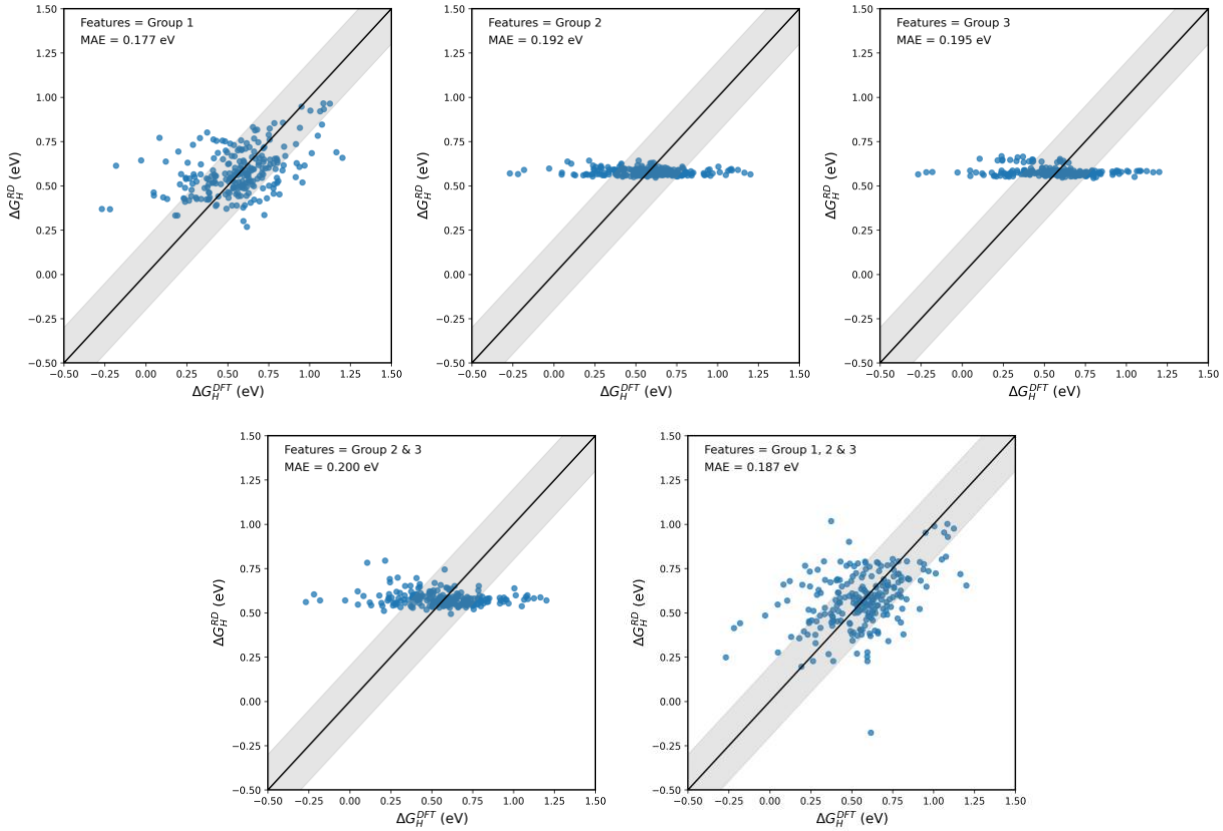

Figure S7: Parity plots illustrating the predictive power of the Ridge Regression (RD) model across various feature groups: Group 1 (top left), Group 2 (top center), Group 3 (top right), combined Groups 2 and 3 (bottom left), and combined Groups 1, 2, and 3 (bottom right). The features of Group 1 alone produce a comparatively low *MAE* of 0.177 eV, signifying adequate predictive accuracy in the absence of DFT-based features. Features from Group 2 and Group 3, both separately and in conjunction, have increased *MAE* values (0.192 eV and 0.200 eV, respectively), with data points deviating from the parity line, signifying limited predictive capability.

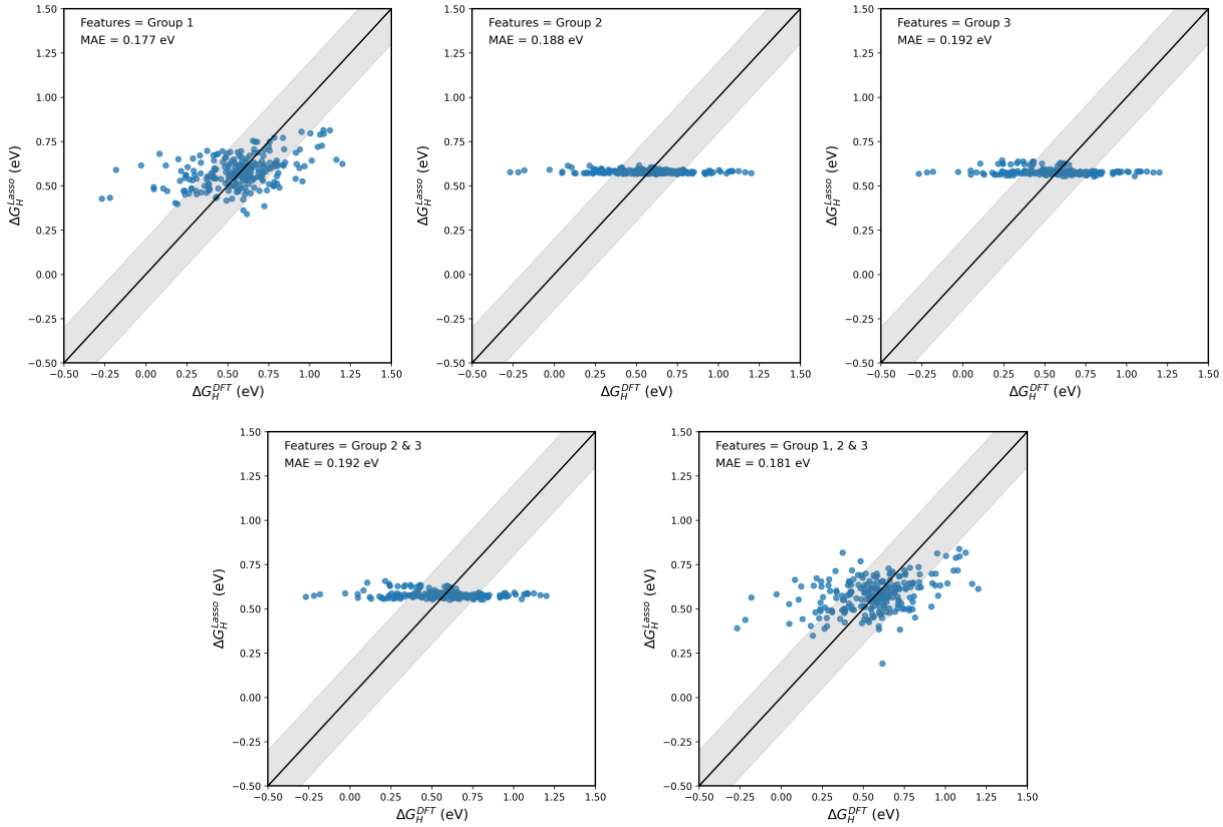

Figure S8: Parity plots illustrating the predictive power of the LASSO regression model across various feature groups: Group 1 (top left), Group 2 (top center), Group 3 (top right), combined Groups 2 and 3 (bottom left), and combined Groups 1, 2, and 3 (bottom right). The features of Group 1 alone produce a comparatively low MAE of 0.177 eV, signifying adequate predictive accuracy in the absence of DFT-based features. Features from Group 2 and Group 3, both separately and in conjunction, have increased MAE values (0.188 and 0.192 eV, respectively), with data points deviating from the parity line, signifying limited predictive capability.

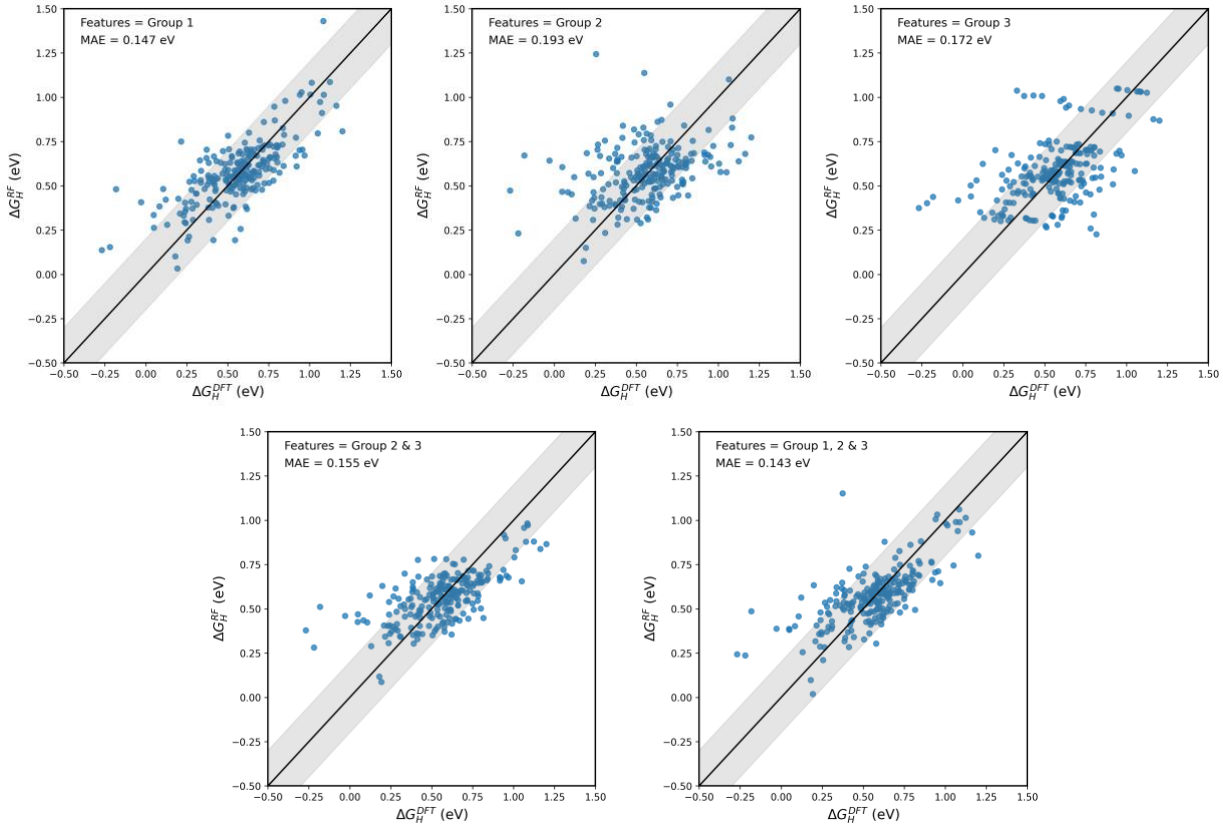

Figure S9: Parity plots illustrating the predictive power of the RFR model utilizing various feature groups: Group 1 (top left), Group 2 (top center), Group 3 (top right), combined Groups 2 and 3 (bottom left), and combined Groups 1, 2, and 3 (bottom right). Group 1 exhibits the low *MAE* of 0.147 eV, indicating robust prediction performance without the use of DFT-based properties. Group 2 and Group 3, independently, yield increased *MAE*s (0.193 eV and 0.172 eV, respectively), signifying reduced predictive power when utilized in individual. Nonetheless, the conjugation of Groups 2 and 3 reduces the *MAE* to 0.155 eV, indicating a moderate enhancement. The incorporation of all three groups (Group 1, 2, and 3) results in a mean absolute error (*MAE*) of 0.143 eV, indicating that the characteristics of Group 1 predominantly enhance the model's accuracy, while Groups 2 and 3 provide minimal nevertheless beneficial enhancements.

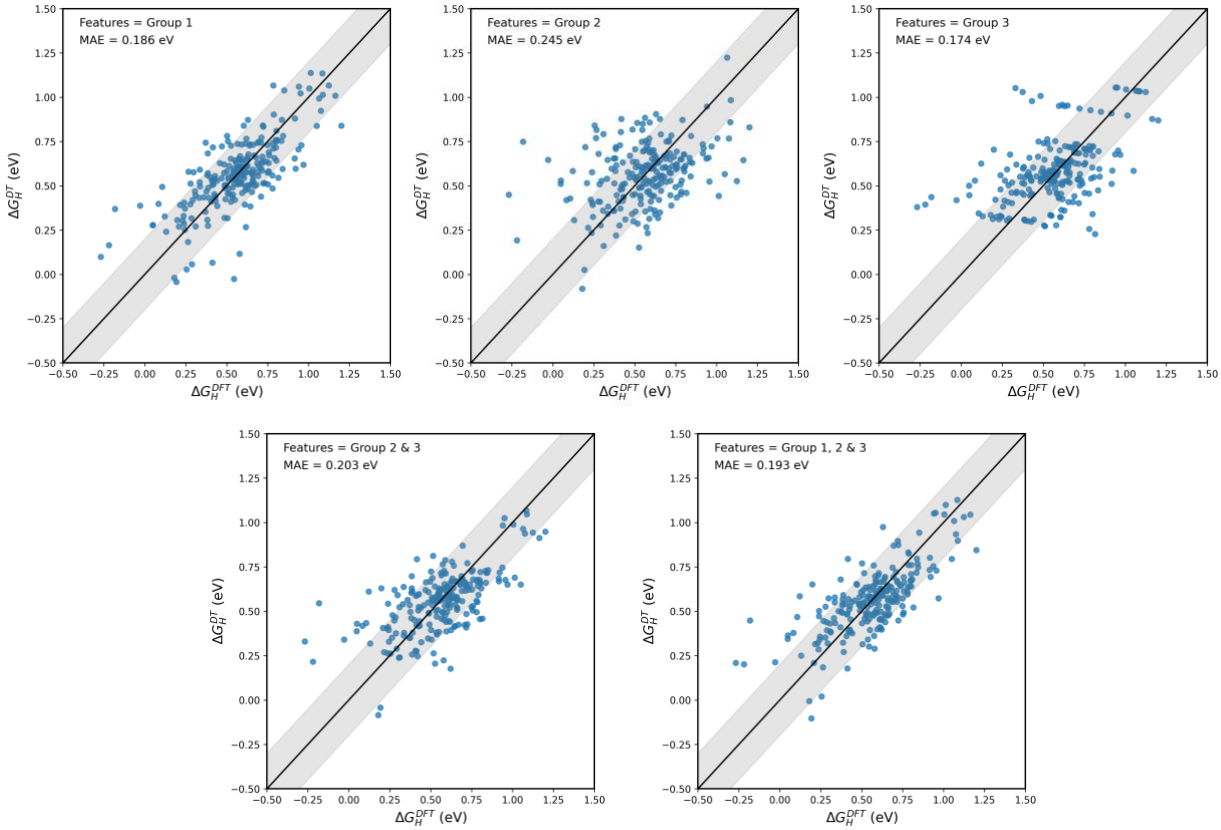

Figure S10: Parity plots demonstrating the predictive power of the DTR model utilizing various feature groups: Group 1 (top left), Group 2 (top center), Group 3 (top right), combined Groups 2 & 3 (bottom left), and combined Groups 1, 2 & 3 (bottom right). Group 1 properties attain a mean absolute error of 0.186 eV, indicating moderate prediction accuracy. The features of Group 2 and Group 3 independently have increased MAEs of 0.245 and 0.174 eV, respectively, indicating diminished predictive power when utilized individually. The conjugation of Groups 2 and 3 produces a MAE of 0.203 eV, whereas the comprehensive feature set with Groups 1, 2, and 3 results in a comparable MAE of 0.193 eV.

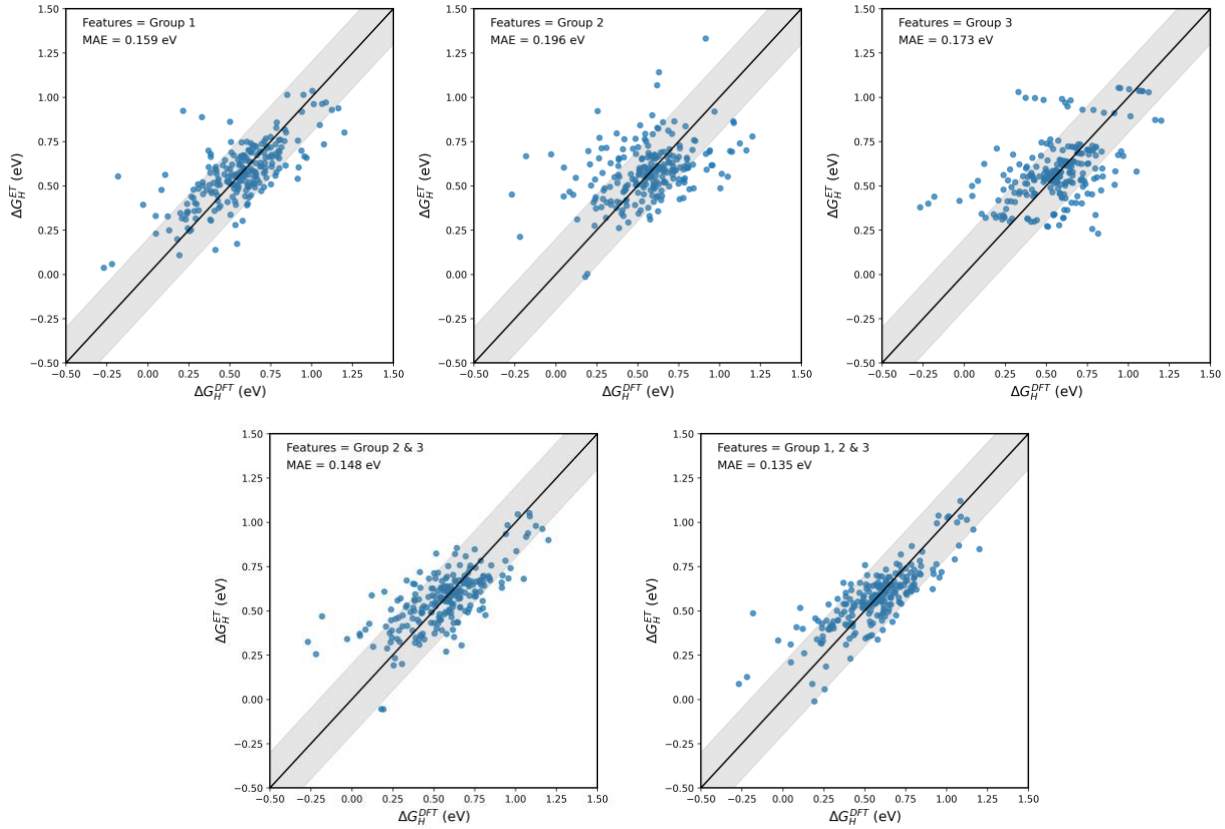

Figure S11: Parity plots illustrating the predictive power of the ETR model utilizing several feature groups: Group 1 (top left), Group 2 (top center), Group 3 (top right), combined Groups 2 & 3 (bottom left), and combined Groups 1, 2 & 3 (bottom right). The model attains an MAE of 0.159 eV using only Group 1 features. Group 2 and Group 3 features independently produce MAEs of 0.196 eV and 0.173 eV, respectively. Combining Groups 2 and 3 yields an MAE of 0.148 eV, whereas utilizing the complete feature set (Groups 1, 2, and 3) achieves the lowest MAE of 0.135 eV. The results indicate that the ETR model gets advantages from all feature groups, attaining optimal performance through the integration of features from Groups 1, 2, and 3.

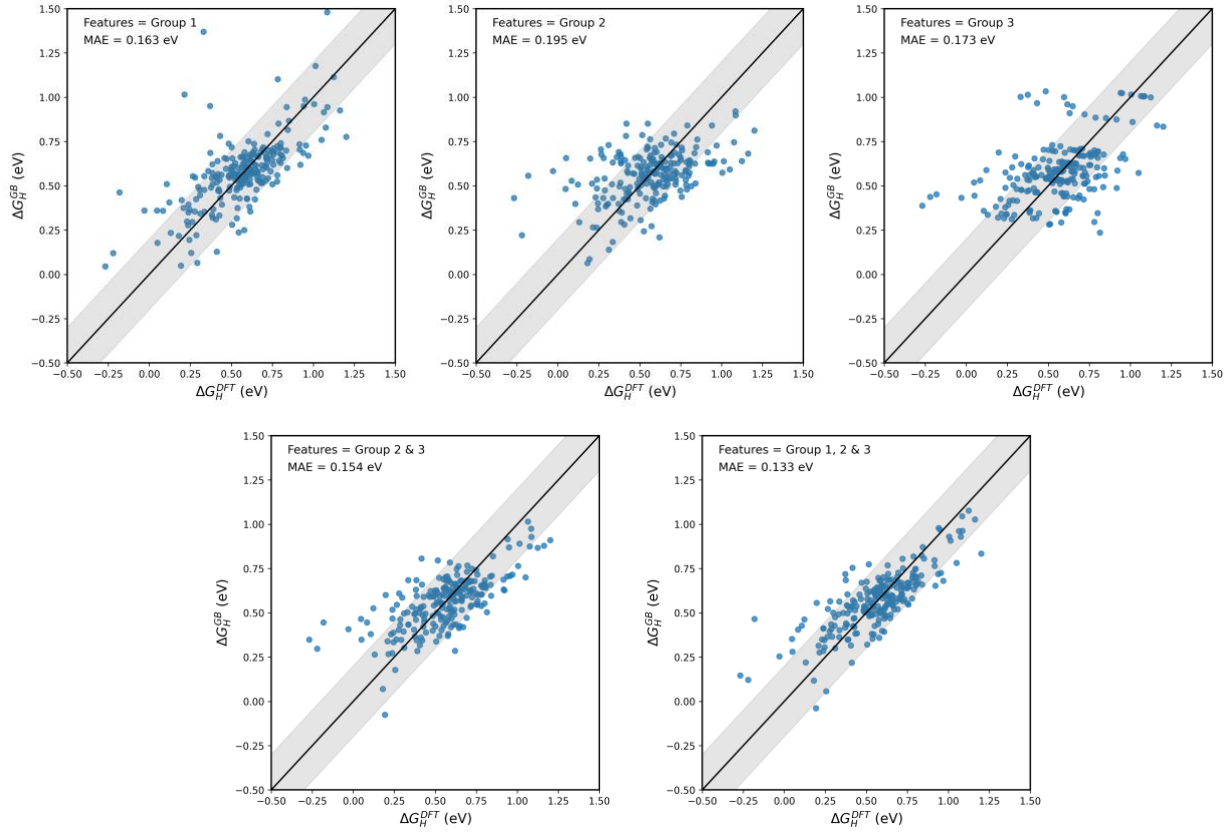

Figure S12: Parity plots illustrating the predictive power of the GBR model utilizing various feature groups: Group 1 (top left), Group 2 (top center), Group 3 (top right), the amalgamation of Groups 2 & 3 (bottom left), and the integration of Groups 1, 2 & 3 (bottom right). The features of Group 1 alone produce an MAE of 0.163 eV. The features of Group 2 and Group 3 independently yield elevated MAEs of 0.195 eV and 0.173 eV, respectively. Integrating Groups 2 and 3 decreases the MAE to 0.154 eV, while employing all feature groups (Groups 1, 2, and 3) attains the minimal MAE of 0.133 eV. The results demonstrate that the GBR model gets advantages from all feature groups, attaining peak performance with the integrated feature sets.

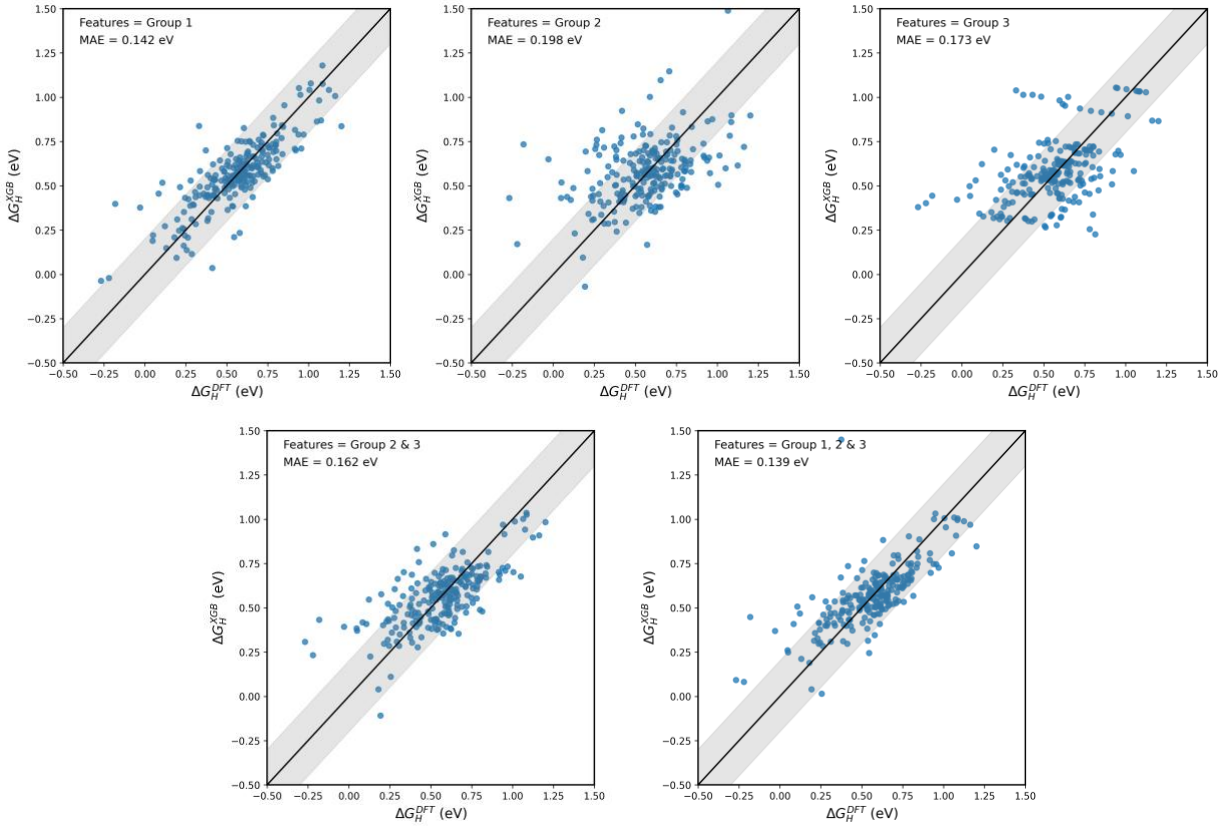

Figure S13: Parity plots illustrating the predictive power of the XGBoost model utilizing various feature groups: Group 1 (top left), Group 2 (top center), Group 3 (top right), combined Groups 2 and 3 (bottom left), and combined Groups 1, 2, and 3 (bottom right). The model attains an MAE of 0.142 eV using only Group 1 features. Group 2 and Group 3 features independently provide higher MAEs of 0.198 eV and 0.173 eV, respectively. The conjugation of Groups 2 and 3 yields an MAE of 0.162 eV, while the utilization of the complete feature set (Groups 1, 2, and 3) offers an enhancement with an MAE of 0.139 eV.

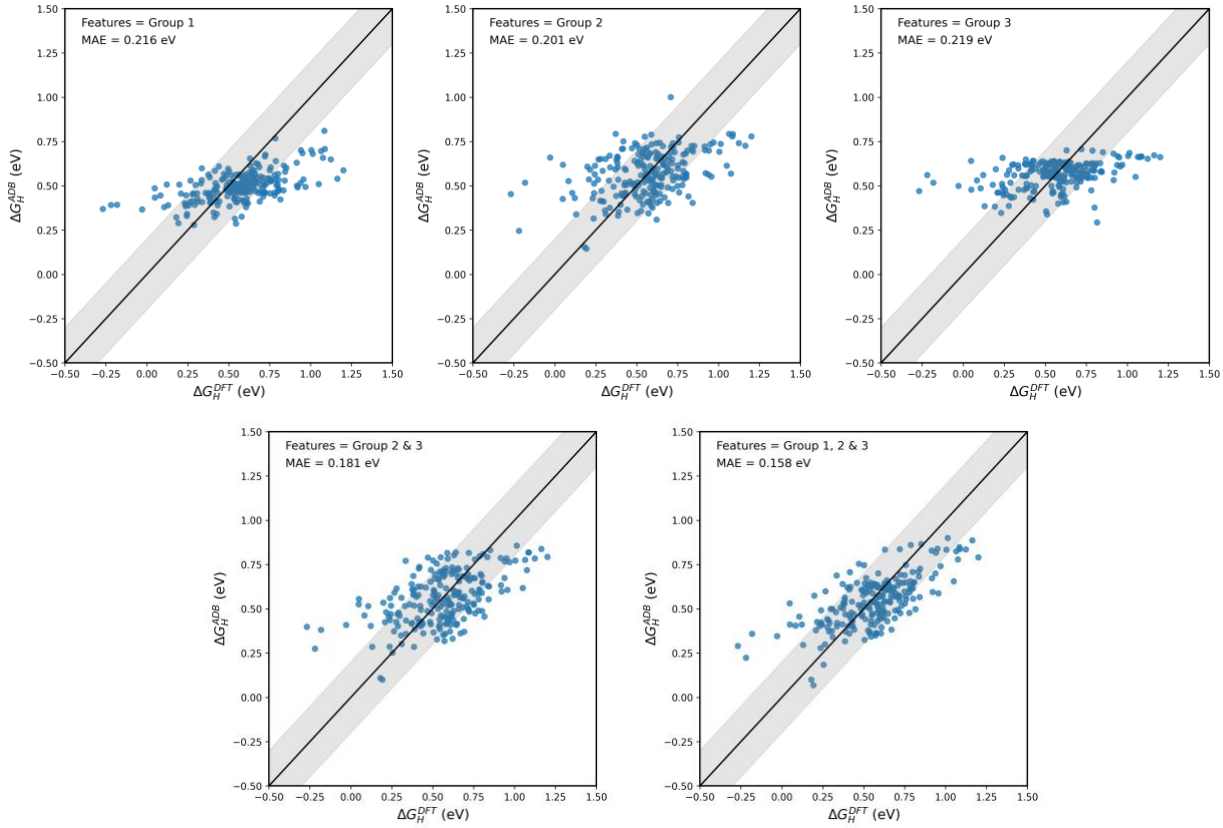

Figure S14: Parity plots illustrating the predictive power of the AdaBoost (ADB) model utilizing various feature groups: Group 1 (top left), Group 2 (top center), Group 3 (top right), combined Groups 2 and 3 (bottom left), and combined Groups 1, 2, and 3 (bottom right). The model attains an MAE of 0.216 eV with only Group 1 features. Features from Group 2 and Group 3 provide individual MAEs of 0.201 eV and 0.219 eV, respectively. The conjugation of Groups 2 and 3 yields an MAE of 0.181 eV, but the incorporation of the complete feature set (Groups 1, 2, and 3) reduces the MAE to 0.158 eV.

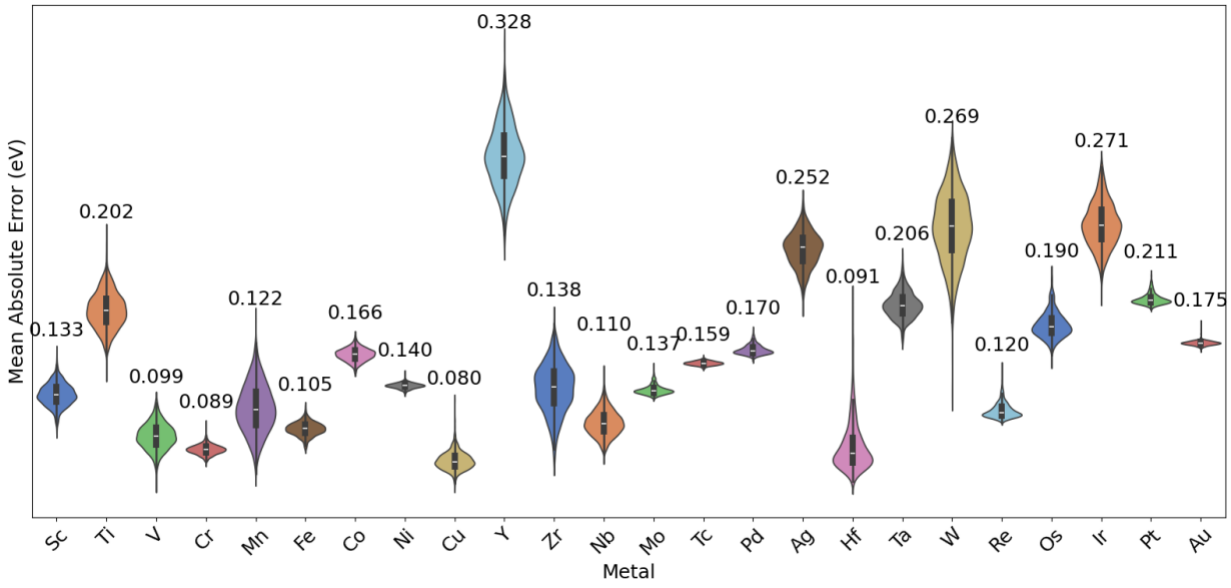

Figure S15: Distribution of MAE for each metal in the one-out experiment, wherein each metal is sequentially excluded from the training set and utilized as the test set. The violin figure illustrates the spread and central tendency of MAE values across 1,000 iterations, where narrower distributions signify more reliable and consistent predictions. Metals such as V, Cr, Ni, and Cu exhibit the lowest average MAE values (0.099, 0.089, 0.140, and 0.080 eV, respectively), indicating that the model demonstrates strong performance with these metals. Conversely, metals like Y, Ag, and W demonstrate relatively increased average MAEs (0.328, 0.252, and 0.269 eV, respectively). This figure illustrates the generalizability of our model among several metals.

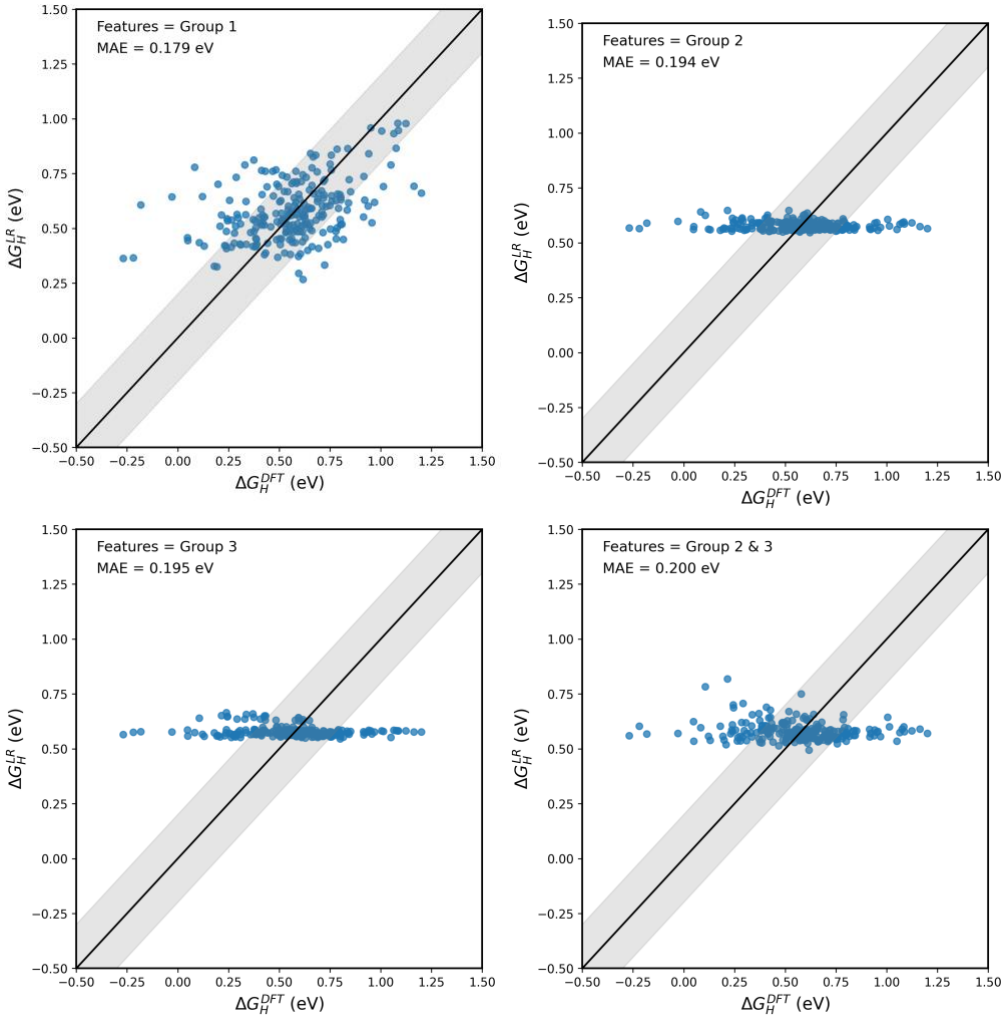

Figure S16: Parity plot showing the correlation of group features for linear regression model for prediction of the target.

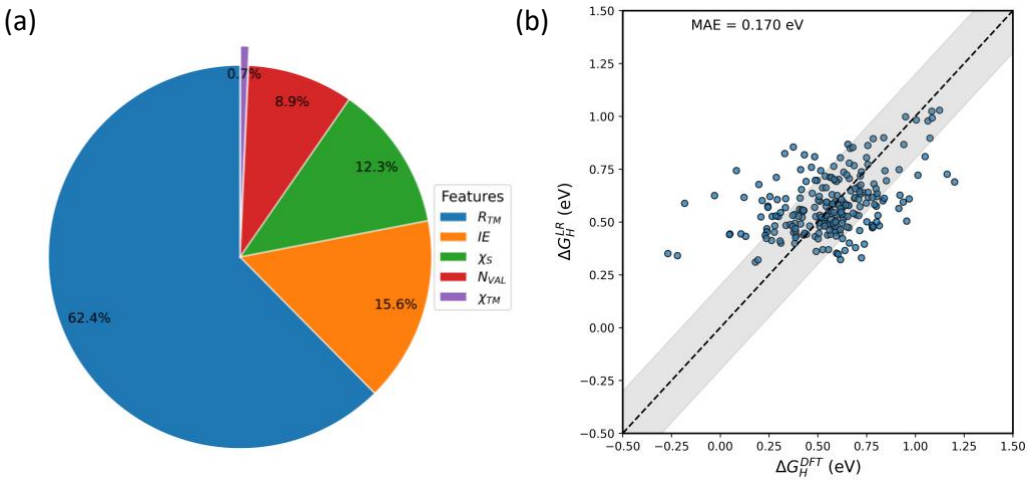

Figure S17: (a) Feature importance analysis for group 1 features and (b) the parity plot using standardized features.

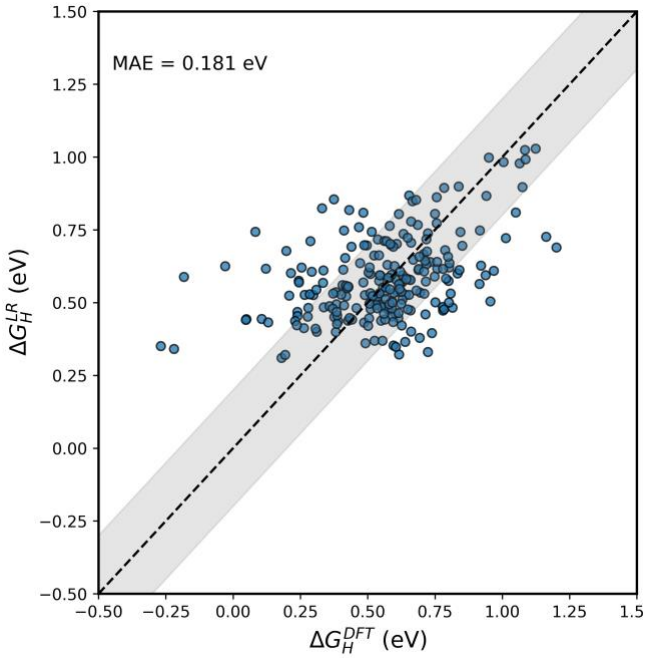

Figure S18: The parity plot using non-standardized features.

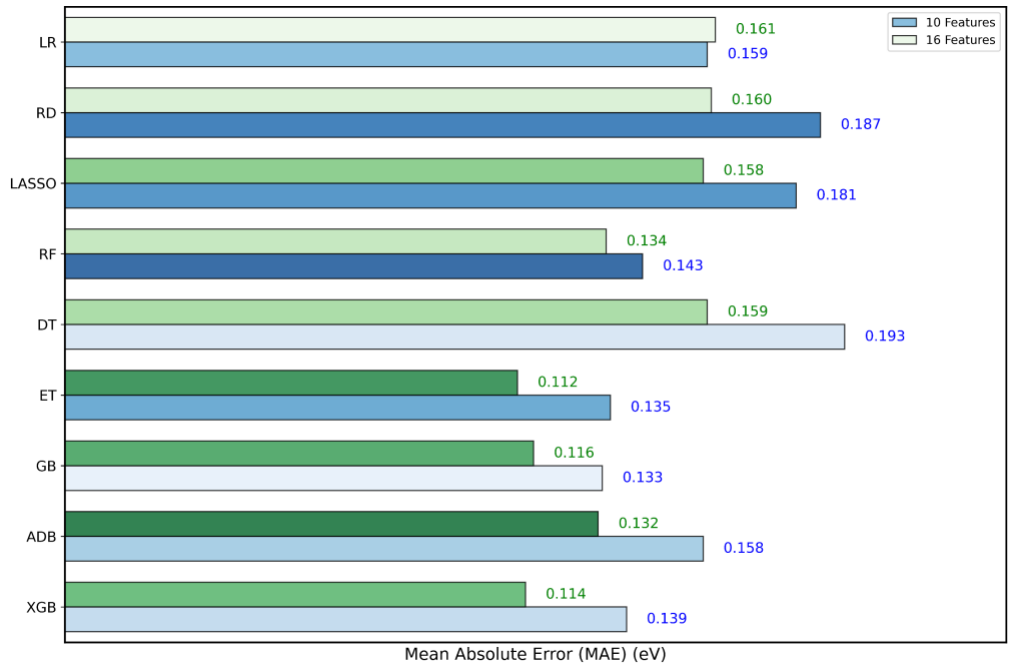

Figure S19: Comparison of MAE among several models utilizing ten features (blue bars) against 16 features (green bars). The performance of each model is quantified in eV, where *MAE* values signify enhanced accuracy. The low performance difference between 10 and 16 features suggests limited advantages from additional features, hence validating our selection of the ten features.

Table S1: Comparison of model performance metrics (MAE, RMSE and R^2) for Group 1, 2 & 3 features using 10-fold cross-validation.

Model	Train MAE_mean	Test MAE_mean	Train RMSE_mean	Test RMSE_mean	Train R^2_mean	Test R^2_mean
LR	0.150	0.159	0.192	0.201	0.381	0.292
RD	0.170	0.187	0.193	0.200	0.353	0.278
LASSO	0.162	0.181	0.207	0.208	0.254	0.221
RF	0.125	0.143	0.167	0.191	0.545	0.432

DT	0.184	0.193	0.214	0.225	0.487	0.394
ET	0.121	0.135	0.201	0.211	0.412	0.376
GB	0.109	0.133	0.124	0.154	0.735	0.715
ADB	0.140	0.158	0.174	0.199	0.489	0.395
XGB	0.133	0.139	0.200	0.216	0.453	0.374

Despite the moderate train-test-set R^2 values of the models (0.22–0.72), this must be understood within the framework of the target-property distribution and the intrinsic error of DFT. The ΔG_H values exhibit a limited range (about –0.3 to 1.2 eV), resulting in minor absolute differences (~0.1–0.15 eV) that lead to significant proportional variances and hence reduced R^2 values. The top-performing models (Gradient Boosting, Extra Trees) produce MAE values ranging from 0.13 to 0.15 eV, aligning with the intrinsic DFT accuracy limit of 0.10 to 0.20 eV for hydrogen adsorption energies. The results confirm that, despite moderate R^2 values, the models attain physically significant prediction performance. Consequently, MAE and RMSE are regarded as more dependable metrics of model accuracy in this context, directly representing absolute errors that are comparable to DFT precision and ensuring practical applicability of our model for catalyst screening.